

# RETARGETING PYRAMID USING DIRECT DECIMATION

Ryosuke Morita<sup>†</sup>, Keiichiro Shirai<sup>#</sup>, and Yuichi Tanaka<sup>†\*</sup>

<sup>†</sup>Graduate School of BASE, Tokyo University of Agriculture and Technology  
Koganei, Tokyo, 184-8588 Japan

Email: morita@msp.lab.tuat.ac.jp, ytnk@cc.tuat.ac.jp

<sup>#</sup>Department of Computer Science and Engineering, Shinshu University

Wakasato, Nagano, 380-8553 Japan

Email: keiichi@shinshu-u.ac.jp

## ABSTRACT

The retargeting pyramid (RP) is a multiscale image pyramid using content-aware image resizing. In the previous implementation of the RP, a two-step interpolation is adopted to obtain the desired resolution. However, this interpolation leads to performance loss for image processing. In this paper, we improve the performance of the RP by replacing the two-step interpolation with a single interpolation using a matrix representation of the bilateral filter and Tikhonov regularization.

**Index Terms**— Retargeting, content-aware image resizing, denoising, retargeting pyramid, Laplacian pyramid, bilateral filter, Tikhonov regularization.

## 1. INTRODUCTION

Multiscale (MS) decomposition of images, e.g., by using wavelet transforms [1], [2], is known as an effective method for analyzing image signals. We can use it in various image processing applications, such as compression, denoising, enhancement, and texture retrieval. As a method for implementing MS decomposition, Laplacian pyramid (LP) method [3] is widely used. The LP performs separable lowpass filterings along both horizontal and vertical directions, followed by the explicit downsampling.

Many images contain diagonal edges as well as horizontal/vertical ones. Therefore, multidirection (MD) decomposition is also beneficial as well as MS decomposition. Without being exhaustive, contourlet [4–7], directionlet [8, 9], and curvelet [10] are key methods for MSMD decomposition based on the traditional MS decomposition. In particular, the contourlet transforms (CTs) are closely related to the LP, and achieve the MSMD decomposition by combining the LP and directional filter banks (DFBs) [11–13].

The retargeting pyramid (RP) [14, 15] has been proposed as an alternative to the LP. It achieves MS decomposition considering the *importance of content* in an image. Furthermore, it can be incorporated with DFBs to realize content-aware MSMD decomposition. The RP replaces low-pass filtering and downsampling in the LP with image retargeting, which is also known as content-aware image resizing [17–27]. Roughly speaking, the explicit low-pass filtering and downsampling approach in the LP is replaced with *implicit* downsampling and filtering by utilizing image retargeting. However, image retargeting in the RP requires a two-step interpolation: It leads to performance loss for image processing.

\*This work was supported in part by JSPS KAKENHI Grant Number 24760288 and MEXT Tenure-Track Promotion Program.

This paper proposes a novel decimation operator for the RP using the bilateral filter (BF) [28]. It replaces the two-step interpolation used in the RP with a single interpolation. In order to further improve the performance of the RP, we use Tikhonov regularization [29] to design the decimation matrix. The improved RP (iRP) using our proposed operator outperforms CTs with conventional pyramid structures in our experiments.

The remaining of this paper is constructed as follows. Section 2 gives a review of the RP. The iRP is introduced in Section 3. Section 4 presents the experimental results for some image processing applications. Finally, Section 5 concludes this paper.

## 2. REVIEW

In this section, we briefly review the previous structure of the RP.

### 2.1. Retargeting Pyramid

Considering an  $H_0 \times W_0$  image  $\mathbf{X}$ , let  $\mathbf{x}^{(0)} \in \mathbb{R}^{H_0 W_0}$  be the vectorized version of  $\mathbf{X}$ . The significances (saliencies) of an image is transformed by retargeting. For the  $K$ -level decomposition, retargeting is performed by  $K_{sig}$  levels, and its output is further transformed by using the LP for  $K_{freq} = K - K_{sig}$  levels. The  $k$ -th level outputs  $\mathbf{x}^{(k+1)}$  and  $\hat{\mathbf{x}}^{(k)}$  in the RP are represented as

$$\mathbf{x}^{(k+1)} = \begin{cases} \mathbf{R}^{(k)} \mathbf{x}^{(k)} & 0 \leq k \leq K_{sig} - 1 \\ \mathbf{L}^{(k)} \mathbf{x}^{(k)} & K_{sig} \leq k \leq K - 1 \end{cases}, \quad (1)$$

$$\hat{\mathbf{x}}^{(k)} = \begin{cases} \mathbf{x}^{(k)} - \mathbf{R}^{*(k)} \mathbf{x}^{(k+1)} & 0 \leq k \leq K_{sig} - 1 \\ \mathbf{H}^{(k)} \mathbf{x}^{(k)} & K_{sig} \leq k \leq K - 1 \end{cases}, \quad (2)$$

where  $\mathbf{x}^{(k+1)}$  indicates a low-pass component,  $\hat{\mathbf{x}}^{(k)}$  is a high-pass component, and  $\mathbf{R}$  is the retargeting operator described in Sec. 2.2.  $\mathbf{L}$  and  $\mathbf{H}$  are the low-pass and high-pass filters, respectively, creating a perfect reconstruction filter bank.  $\mathbf{R}$  contains low-pass filtering and downsampling implicitly, and  $\mathbf{R}^*$  is the pseudo inverse operator of  $\mathbf{R}$ . Note that  $\mathbf{R}^* \mathbf{R} \neq \mathbf{I}$  where  $\mathbf{I}$  is an identity matrix. In the previous RP [14, 15], the structure is designed as shown in Fig. 1, and the retargeting operator  $\mathbf{R}$  consists of two independent operations:

$$\mathbf{R} = \mathbf{\Lambda} \mathbf{\Phi}, \quad (3)$$

where  $\mathbf{\Lambda}$  is uniform bicubic scaling, and  $\mathbf{\Phi}$  is the warping operation which deforms original pixels while keeping the original size of  $k$ -th level input image.

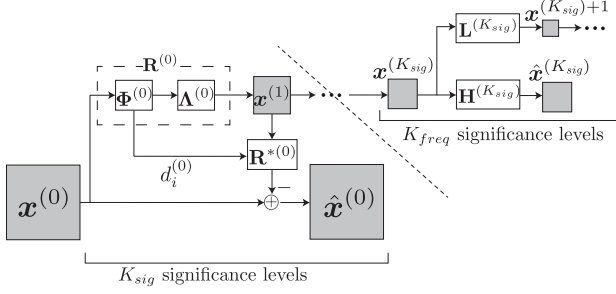


Fig. 1. Retargeting Pyramid.

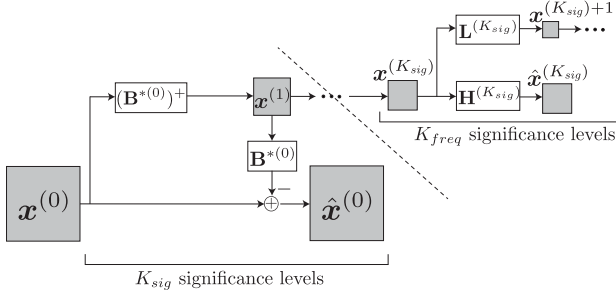


Fig. 2. Improved Retargeting Pyramid.

## 2.2. Retargeting in the RP

The algorithm of image retargeting used in the RP is similar to a mesh warping method described in [20]. Let  $\mathbf{p}$  be the original pixel position  $\mathbf{p} \in \mathbb{R}^2 \mid (0, 0) \leq \mathbf{p} \leq (H_0 - 1, W_0 - 1)$ . The pixel position after mesh deformation is defined as

$$\mathbf{p}'(i) = \mathbf{p}(i) + \mathbf{d}(i), \quad (4)$$

where  $i$  is a pixel index and  $\mathbf{d}$  is a displacement vector of the mesh. To obtain the optimized mesh, significant regions are extracted by using a significance map. In the RP, the significance is represented as a weight in a similar way in [20]:

$$\mathbf{W} = \frac{1}{2} \left( \frac{1}{\max(\mathbf{W}_\alpha)} \mathbf{W}_\alpha + \mathbf{W}_\beta \right), \quad (5)$$

where  $\mathbf{W}_\alpha = \|\nabla \mathbf{X}\|_2$  is the  $l_2$ -norm of the gradient, and  $\mathbf{W}_\beta$  is a saliency map which is given in [16]. In order to optimize a mesh based on (5), we consider the following cost function:

$$E(\mathbf{p}', s_f, l_{ij}) = E_m(\mathbf{p}') + \gamma \{E_u(\mathbf{p}', s_f) + E_l(\mathbf{p}', l_{ij})\}, \quad (6)$$

where  $\gamma$  is the weight for  $E_l$ ,  $s_f$  is the scale factor of a quad face between  $\mathbf{p}$  and  $\mathbf{p}'$ , and  $l_{ij}$  is the length ratio of the quad edges. In (6),  $E_m$  is used to stretch meshes based on the value of  $\mathbf{W}$ ,  $E_u$  keeps the shapes of original mesh faces, and  $E_l$  prevents edges from being bent among vertices (pixels). The optimal mesh can be obtained by updating  $\mathbf{p}'$  iteratively.

## 3. DIRECT DECIMATION FOR IMPROVED RP

A novel decimation operator for the RP is proposed in this section. The flow of our proposed iRP is outlined in Fig. 2. It is constructed by replacing the two-step interpolation in the previous RP with a single interpolation that can be obtained by modifying the BF. The iRP, thereby, is expected to be superior in edge preserving.

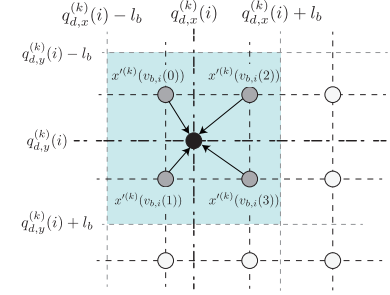
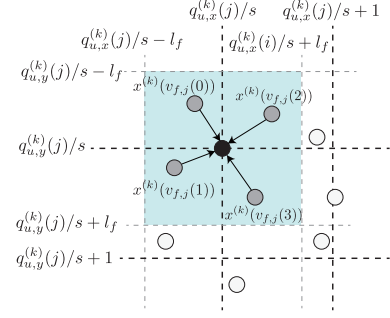


Fig. 3.  $v_{f,j}(n)$  and  $v_{b,i}(m)$  of the modified BF. Where blue regions represent filter sizes. Top:  $v_{f,j}(n)$ . Bottom:  $v_{b,i}(m)$ . Black dots represent pixels to be interpolated and gray ones are available pixels for interpolation.

## 3.1. Bilateral Filter for the iRP

The  $k$ -th level outputs in the iRP are calculated as

$$\mathbf{x}^{(k+1)} = \begin{cases} (\mathbf{B}^{*(k)})^+ \mathbf{x}^{(k)} & 0 \leq k \leq K_{sig} - 1 \\ \mathbf{L}^{(k)} \mathbf{x}^{(k)} & K_{sig} \leq k \leq K - 1 \end{cases}, \quad (7)$$

$$\hat{\mathbf{x}}^{(k)} = \begin{cases} \mathbf{x}^{(k)} - \mathbf{B}^{*(k)} \mathbf{x}^{(k+1)} & 0 \leq k \leq K_{sig} - 1 \\ \mathbf{H}^{(k)} \mathbf{x}^{(k)} & K_{sig} \leq k \leq K - 1 \end{cases}, \quad (8)$$

where  $\mathbf{B}^{*(k)} \in \mathbb{R}^{H_k W_k s^2 \times H_k W_k s^2}$  contains filter coefficients of the modified BF in each row. Moreover,  $H_k$  and  $W_k$  are the height and the width of the  $k$ -th level input image, respectively, and  $s (< 1)$  is the scaling factor.  $(\mathbf{B}^{*(k)})^+$  is introduced in Sec. 3.3. Note that the original BF is not directly applicable to irregularly placed pixels such as the warped image by  $\Phi$ . In order to apply the BF to the RP, it should be modified.

## 3.2. Derivation of $\mathbf{B}^{*(k)}$

First we calculate the upsampling matrix  $\mathbf{B}^{*(k)}$ . Before calculating  $\mathbf{B}^{*(k)}$ , the following preprocessing is performed:

$$\mathbf{x}'^{(k+1)} = \mathbf{B}^{(k)} \mathbf{x}^{(k)}, \quad (9)$$

where  $\mathbf{B}^{(k)} \in \mathbb{R}^{H_k W_k s^2 \times H_k W_k}$  contains filter coefficients of the modified BF in each row. To calculate  $\mathbf{B}^{(k)}$ , a pre-retargeted image  $\mathbf{r}_f$  is calculated by

$$\mathbf{r}_f = \mathbf{R}^{(k)} \mathbf{x}^{(k)}. \quad (10)$$

Let  $\mathbf{q}_{u,x}^{(k)}$  and  $\mathbf{q}_{u,y}^{(k)}$  be vectors containing coordinates of  $\mathbf{x}'^{(k+1)}$ , respectively. The filter coefficients of the modified BF are represented

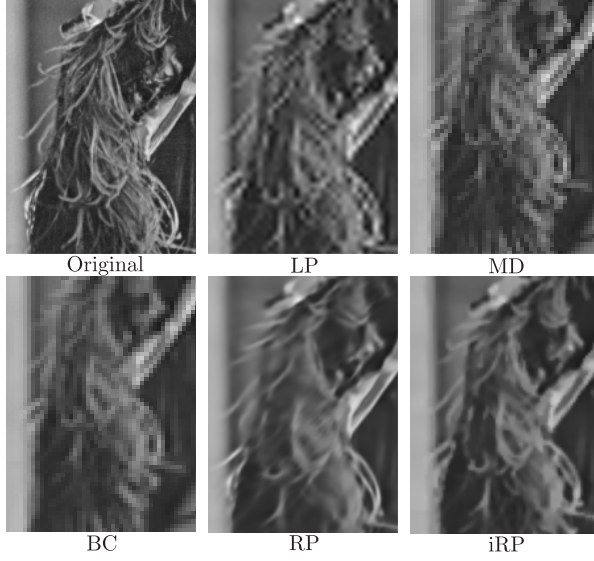


**Fig. 4.** Enlarged portions of approximated *Lena* from downsampled  $64 \times 64$  images.

as follows:

$$B^{(k)}(j, v_{f,j}(n)) = \frac{w_{f,s}(j, n)w_{f,i}(j, n)}{\sum_{n \in n_{\text{num}}} w_{f,s}(j, n)w_{f,i}(j, n)}, \quad (11)$$

$$w_{f,s}(j, n) = \exp\left(-\frac{d_{f,x}(j, n)^2 + d_{f,y}(j, n)^2}{2\sigma_1^2}\right), \quad (12)$$

$$w_{f,i}(j, n) = \exp\left(-\frac{(r_f(j) - x^{(k)}(v_{f,j}(n)))^2}{2\sigma_2^2}\right), \quad (13)$$

$$d_{f,x}(j, n) = q_{d,x}^{(k)}(v_{f,j}(n)) - q_{u,x}^{(k)}(j)/s, \quad (14)$$

$$d_{f,y}(j, n) = q_{d,y}^{(k)}(v_{f,j}(n)) - q_{u,y}^{(k)}(j)/s, \quad (15)$$

where  $j$  is a pixel index of  $\mathbf{x}'^{(k+1)}$  in (9) and  $\mathbf{v}_{f,j}$  contains pixel indices in the support region of the BF, which satisfies both (16) and (17):

$$q_{u,x}^{(k)}(j)/s - l_f \leq q_{d,x}^{(k)}(v_{f,j}(n)) \leq q_{u,x}^{(k)}(j)/s + l_f, \quad (16)$$

$$q_{u,y}^{(k)}(j)/s - l_f \leq q_{d,y}^{(k)}(v_{f,j}(n)) \leq q_{u,y}^{(k)}(j)/s + l_f, \quad (17)$$

in which  $l_f$  is the filter size of  $\mathbf{B}^{(k)}$  and  $n$  is the index of  $\mathbf{v}_{f,j}$  illustrated in Fig. 3. Additionally,  $n_{\text{num}}$  in (11) is the number of elements in  $\mathbf{v}_{f,j}$ ,  $\mathbf{q}_{d,x}^{(k)}$  and  $\mathbf{q}_{d,y}^{(k)}$  are vectors containing coordinates of  $\mathbf{p}'$  in (4), respectively, and  $\sigma_1$  and  $\sigma_2$  are standard deviations of Gaussian distributions.

$\mathbf{B}^{*(k)} \in \mathbb{R}^{H_k W_k \times H_k W_k s^2}$  in (8) can be similarly obtained as follows. First, a blurred image  $\mathbf{r}_b$  is calculated as

$$\mathbf{r}_b = \mathbf{G}^{(k)} \mathbf{x}^{(k)}, \quad (18)$$

where  $\mathbf{G}^{(k)}$  is the Gaussian filtering operator. After that,  $\mathbf{B}^{*(k)}$  is

Parameters	$\sigma_1$	$\sigma_2$	$l_f$	$l_b$	$\lambda$
iRP	5	8	2	5	0.04
CT-iRP	20	30	3	8	0.04

**Table 2.** Performance comparison of linear approximated images from higher decomposition level: PSNR (dB)

$K_{sig} = 1$ (reconstruction from $128 \times 128$ )					
Image	LP	MD	BC	RP	iRP
<i>Monarch</i>	28.35	25.69	27.27	28.36	<b>34.50</b>
<i>Pepper</i>	31.99	29.33	31.05	32.39	<b>36.72</b>
<i>Lena</i>	31.81	29.15	31.10	32.66	<b>35.95</b>
$K_{sig} = 2$ (reconstruction from $64 \times 64$ )					
Image	LP	MD	BC	RP	iRP
<i>Monarch</i>	22.30	20.56	21.60	22.11	<b>29.65</b>
<i>Pepper</i>	26.13	24.53	25.72	26.41	<b>32.12</b>
<i>Lena</i>	26.18	24.76	25.97	26.72	<b>31.98</b>

obtained as

$$B^{*(k)}(i, v_{b,i}(m)) = \frac{w_{b,s}(i, m)w_{b,i}(i, m)}{\sum_{m \in m_{\text{num}}} w_{b,s}(i, m)w_{b,i}(i, m)}, \quad (19)$$

$$w_{b,s}(i, m) = \exp\left(-\frac{d_{b,x}(i, m)^2 + d_{b,y}(i, m)^2}{2\sigma_1^2}\right), \quad (20)$$

$$w_{b,i}(i, m) = \exp\left(-\frac{(r_b(i) - x'^{(k+1)}(v_{b,i}(m)))^2}{2\sigma_2^2}\right), \quad (21)$$

$$d_{b,x}(i, m) = q_{d,x}^{(k)}(i) - q_{u,x}^{(k)}(v_{b,i}(m))/s, \quad (22)$$

$$d_{b,y}(i, m) = q_{d,y}^{(k)}(i) - q_{u,y}^{(k)}(v_{b,i}(m))/s, \quad (23)$$

where  $i$  is shown in (4) and  $\mathbf{v}_{b,i}$  contains pixel indices in the support region of the BF. It satisfies both (24) and (25):

$$q_{d,x}^{(k)}(i) - l_b \leq q_{u,x}^{(k)}(v_{b,i}(m))/s \leq q_{d,x}^{(k)}(i) + l_b, \quad (24)$$

$$q_{d,y}^{(k)}(i) - l_b \leq q_{u,y}^{(k)}(v_{b,i}(m))/s \leq q_{d,y}^{(k)}(i) + l_b, \quad (25)$$

where  $l_b$  is the filter size of  $\mathbf{B}^{*(k)}$  and  $m$  is the pixel index of  $\mathbf{v}_{b,i}$ .  $v_{b,i}(m)$  is also illustrated in Fig. 3. Furthermore,  $m_{\text{num}}$  in (19) is the number of elements in  $\mathbf{v}_{b,i}$ .

### 3.3. Derivation of $(\mathbf{B}^{*(k)})^+$ using Tikhonov Regularization

Tikhonov regularization [29] is further applied to yield a decimation matrix.  $(\mathbf{B}^{*(k)})^+$  in (7) can be obtained by solving the following least squares problem:

$$\|\mathbf{B}^{*(k)} \mathbf{x}^{(k+1)} - \mathbf{x}^{(k)}\|_2^2 + \lambda \|\mathbf{x}^{(k+1)}\|_2^2, \quad (26)$$

where  $\lambda$  is an arbitrary weight. As a result,  $(\mathbf{B}^{*(k)})^+$  is obtained as

$$(\mathbf{B}^{*(k)})^+ = ((\mathbf{B}^{*(k)})^T \mathbf{B}^{*(k)} + \lambda \mathbf{I})^{-1} (\mathbf{B}^{*(k)})^T. \quad (27)$$

## 4. EXPERIMENTAL RESULTS

In this section, we validate our proposed iRP by applying it to a couple of image processing applications. We used three  $256 \times 256$

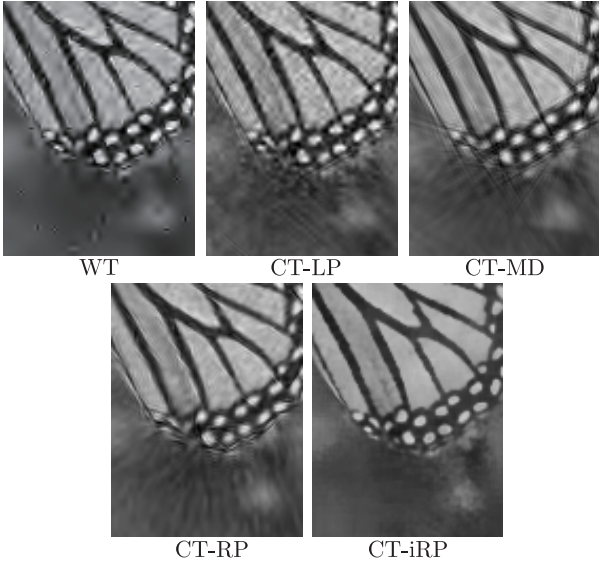


Fig. 5. Enlarged portions of denoised *Monarch* with  $\sigma = 20$ .

grayscale images of *Monarch*, *Pepper*, and *Lena* as the test images. As the conventional methods, we use the discrete wavelet transform (WT), bicubic resizing (BC) and pyramid in [4] (MD). For the WT and the low-pass filter for the LP, the well-known biorthogonal 9/7 filter set is used. In our implementation, The size and the standard deviation of the Gaussian filter are  $3 \times 3$  and  $\sigma = 0.75$ , respectively. Additionally, parameters for the iRP are shown in Table 1.

#### 4.1. Linear Approximation from Higher Decomposition Level

We measured the performance of the iRP by reconstructing images from their low-resolution components, i.e., coefficients in high-pass counterpart were zeroed out. We approximated the images after both one and two-level decompositions. For the RP and the iRP, we set  $K_{sig} = \{1, 2\}$ ,  $K_{freq} = 0$ , and  $\gamma = 0.2$ . Other than MS decomposition pyramids, bicubic scaling is performed for a comparison. First, the image is downsampled by bicubic scaling and it is interpolated back to the original resolution. We use the `imresize` function in MATLAB for bicubic scaling. Table 2 provides the performance comparison of linear approximation. Clearly, the iRP has the best performance for all test images. The approximated portions of *Lena* are presented in Fig. 4. Since the BF preserves edges, the reconstructed image with the iRP has fewer artifacts than others.

#### 4.2. Image Denoising

Here, we introduce the performance of the CT based on the iRP (referred to CT-iRP) by applying it to image denoising. It can be obtained by replacing a pyramid in the CT with the iRP and directional subbands are calculated as

$$\hat{\mathbf{y}}^{(k)} = \mathbf{D}_n^{(k)} \hat{\mathbf{x}}^{(k)}, \quad (28)$$

where  $\hat{\mathbf{y}}^{(k)}$  and  $\mathbf{D}_n^{(k)}$  are directional subbands and the  $k$ -th level transform by DFBs [11–13] with  $2^n$  subbands, respectively. For comparing the pure performance of pyramid structures, we choose the simple hard-thresholding method. We select a threshold of  $3\sigma$ , where  $\sigma$  is the standard deviation of noise. Furthermore, redundancies of all CTs are set to about 1.33. There were  $\{32, 16, 16, 0,$

Table 3. Performance comparison for image denoising: PSNR (dB)

<i>Monarch</i>						
$\sigma$	5	10	15	20	25	30
WT	<b>34.88</b>	30.02	27.34	25.55	24.28	23.81
CT-LP	32.49	28.38	26.27	24.85	23.77	22.93
CT-MD	31.87	28.24	26.53	25.48	24.65	24.03
CT-RP	33.47	29.43	27.19	25.72	24.66	23.81
CT-iRP	33.21	<b>30.84</b>	<b>28.89</b>	<b>27.21</b>	<b>25.70</b>	<b>24.21</b>
<i>Pepper</i>						
$\sigma$	5	10	15	20	25	30
WT	<b>35.40</b>	31.14	28.62	26.91	25.69	24.67
CT-LP	33.55	30.02	27.94	26.52	25.43	24.55
CT-MD	33.32	30.60	29.16	28.06	27.20	26.45
CT-RP	34.97	31.38	29.19	27.73	26.68	25.83
CT-iRP	33.60	<b>31.40</b>	<b>30.18</b>	<b>29.16</b>	<b>28.05</b>	<b>26.47</b>
<i>Lena</i>						
$\sigma$	5	10	15	20	25	30
WT	<b>35.10</b>	30.79	28.45	26.84	25.65	24.66
CT-LP	33.44	29.86	27.93	26.65	25.65	24.92
CT-MD	33.41	30.27	28.81	27.86	27.09	26.43
CT-RP	34.94	31.27	29.33	28.07	27.13	26.37
CT-iRP	33.62	<b>31.42</b>	<b>30.20</b>	<b>29.22</b>	<b>27.98</b>	<b>26.58</b>
Noisy image	34.15	28.14	24.59	22.12	20.21	18.58

$0$  directional subbands for the CT with the LP [5] (referred to as CT-LP),  $\{32, 16, 8, 4, 4\}$  for the CT with the improved pyramid structure [4] (referred to as CT-MD), and  $\{8, 16, 8, 4, 4\}$  for the CT-RP [14, 15] and the CT-iRP from fine to coarse scale. The numbers for the CT-LP and the CT-MD were set as those reported by the original researchers. The same filters as those in the original research on the CT [4, 5], e.g., PKVA 2-D filter bank [13], were used. Table 3 summarizes the performance of denoising. It shows that the CT-iRP always outperforms the CT-LP and all methods within  $5 \leq \sigma \leq 30$  for all test images. The enlarged portions of denoised images of *Monarch* are shown in Fig. 5. It shows distortions that cover up the whole images due to the DFB decomposition are reduced by using the CT-iRP. In addition, the CT-iRP preserves edges as shown in white dots in wings.

## 5. CONCLUSION

In this paper, we propose a novel decimation operator for the retargeting pyramid. We replace the two-step interpolation in the previous RP with a single interpolation using the customized bilateral filter. Furthermore, the decimation operator is improved by using Tikhonov regularization. In our experimental results, the RP using the proposed method outperformed conventional MSMD decompositions for a few image processing applications. Our future work includes reducing the computational complexity and investigating a method to compress side information of mesh in order to apply the iRP to image coding.

## 6. REFERENCES

- [1] M. Vetterli and J. Kovačević, *Wavelets and Subband Coding*, Prentice Hall, NJ, 1995.
- [2] G. Strang and T. Q. Nguyen, *Wavelets and Filter Banks*, Wellesley-Cambridge, MA, 1996.

- [3] P. Burt and E. Adelson, "The Laplacian pyramid as a compact image code," *IEEE Trans. Commun.*, vol. 31, no. 4, pp. 532-540, 1983.
- [4] Y. Lu and M. N. Do, "A new contourlet transform with sharp frequency localization," in *Proc. ICIP'06*, 2006, pp. 1629-1632.
- [5] M. N. Do and M. Vetterli, "The contourlet transform: an efficient directional multiresolution image representation," *IEEE Trans. Image Process.*, vol. 14, no. 12, pp. 2091-2106, 2005.
- [6] Y. Lu and M. N. Do, "CRISP-contourlet: a critically sampled directional multi resolution image representation," in *Proc. SPIE Conf. on Wavelet Applications in Signal and Image Processing*, 2003, pp. 655-665.
- [7] A. L. Da Cunha, J. Zhou, and M. N. Do, "The nonsubsampling contourlet transform: Theory, design, and applications," *IEEE Trans. Image Process.*, vol. 15, no. 10, pp. 3089-3101, 2006.
- [8] V. Velisavljević, B. Beferull-Lozano, M. Vetterli, and P. L. Dragotti, "Directionlets: Anisotropic multi-directional representation with separable filtering," *IEEE Trans. Signal Process.*, vol. 15, no. 7, pp. 1916-1933, 2006.
- [9] V. Velisavljević, B. Beferull-Loano, and M. Vetterli, "Space-frequency quantization for image compression with directionlets," *IEEE Trans. Signal Process.*, vol. 16, no. 7, pp. 1761-1773, 2007.
- [10] E. Candès and D. L. Donoho, "Curvelets — a surprisingly effective nonadaptive representation for objects with edges," in *Curves and Surfaces Fitting*, A. Cohen, C. Rabut, and L. L. Schumaker, Eds. Vanderbilt University Press, Saint-Malo, 1999.
- [11] R. H. Bamberger and M. J. T. Smith, "A filter bank for the directional decomposition of images: theory and design," *IEEE Trans. Image Process.*, vol. 40, no. 4, pp. 1424-1431, 2004.
- [12] S.-I. Park, M. J. T. Smith, and R. M. Mersereau, "Improved structures of maximally decimated directional filter banks for spatial image analysis," *IEEE Trans. Image Process.*, vol. 40, no. 4, pp. 1424-1431, 2004.
- [13] S. M. Phoong, C. W. Kim, P. P. Vaidyanathan, and R. Ansari, "A new class of two-channel biorthogonal filter banks and wavelet bases," *IEEE Trans. Signal Process.*, vol. 43, no. 3, pp. 649-665, 1995.
- [14] Y. Tanaka and K. Shirai, "Directional image decomposition using retargeting pyramid," in *Proc. APSIPA ASC 2012*, 2012.
- [15] Y. Tanaka and K. Shirai, "Scalable image representation using improved retargeting pyramid," in *Proc. ICASSP'13*, 2013, pp. 2232-2236.
- [16] L. Itti, C. Koch, and E. Niebur, "A model of saliency-based visual attention for rapid scene analysis," *IEEE Trans. Pattern Anal. Mach. Intell.*, vol. 20, no. 11, pp. 1254-1259, 1998.
- [17] S. Avidan and A. Shamir, "Seam Carving for content-aware image resizing," *ACM Trans. Graph.*, vol. 26, no. 3, 2007.
- [18] M. Rubinstein, A. Shamir, and S. Avidan, "Improved seam carving for video retargeting," *ACM Trans. Graph.*, vol. 27, no. 3, 2008.
- [19] L. Wolf, M. Guttmann and D. Cohen-Or, "Non-homogeneous content-driven video retargeting," in *Proc. ICCV'07*, 2007.
- [20] Y. Wang, C.-L. Tai, O. Sorkine, and T.-Y. Lee, "Optimized scale-and-stretch for image retargeting," *ACM Trans. Graph.*, vol. 27, no. 5, 2008.
- [21] B. Chen and P. Sen, "Video carving," in *IEEE Proc. Eurographics.*, 2008.
- [22] Z. Li, P. Ishwar, and J. Konrad, "Video condensation by ribbon carving," *IEEE Trans. Image Process.*, vol. 18, no. 11, pp. 2572-2583, 2009.
- [23] Y. Guo, F. Liu, J. Shi, Z. H. Zhou, and M. Gleicher, "Image retargeting using mesh parametrization," *IEEE Trans. Multimedia.*, vol. 11, no. 5, pp. 856-867, 2009.
- [24] Y. Pritch, E. Kav-Venaki, and S. Peleg, "Shift-map image editing," in *Proc. ICCV'09*. IEEE, pp. 151-158, 2009.
- [25] D. Domingues, A. Alahi, and P. Vandergheynst, "Stream carving: An adaptive seam carving algorithm," in *Proc. ICIP' 10*, 2010.
- [26] X. Fan, X. Xie, H. Q. Zhou, and W. Y. Ma, "Looking into video frames on small displays," in *Proc. 11th ACM International Conference on Multimedia*. ACM, pp. 247-250, 2003.
- [27] P. Krähenbühl, M. Lang, A. Hornung, and M. Gross, "A system for retargeting of streaming video", *ACM Trans. Graph.*, vol. 28, no. 5, 2009.
- [28] C. Tomasi and R. Manduchi, "Bilateral filter for gray and color images," in *Proc. International Conference on Computer Vision*, pp.839-846, 1998.
- [29] Tikhonov A. N. and V. Ya Arsenin, "Solutions of ill-posed problems." WH Winston, Washington, DC 330, 1977.